11108 *Inorg. Chem.* **2009**, *48*, 11108–11113
DOI: 10.1021/ic901493j

Inorganic Chemistry
Article

Synthesis, Structure, and Bonding in $K_{12}Au_{21}Sn_4$. A Polar Intermetallic Compound with Dense Au_{20} and Open $AuSn_4$ Layers

Bin Li,† Sung-Jin Kim, Gordon J. Miller, and John D. Corbett*

Ames Laboratory−DOE and Department of Chemistry, Iowa State University, Ames, Iowa 50011.
† Present address: Wildcat Discovery Technologies, Inc., 6985 Flanders Drive, San Diego, CA 92121.

Received July 27, 2009

The new phase $K_{12}Au_{21}Sn_4$ has been synthesized by direct reaction of the elements at elevated temperatures. Single crystal X-ray diffraction established its orthorhombic structure, space group *Pmmn* (No. 59), $a = 12.162(2)$; $b = 18.058(4)$; $c = 8.657(2)$ Å, $V = 1901.3(7)$ Å^3, and $Z = 2$. The structure consists of infinite puckered sheets of vertex-sharing gold tetrahedra (Au_{20}) that are tied together by thin layers of alternating four-bonded-Sn and -Au atoms ($AuSn_4$). Remarkably, the dense but electron-poorer blocks of Au tetrahedra coexist with more open and saturated Au−Sn layers, which are fragments of a zinc blende type structure that maximize tetrahedral heteroatomic bonding outside of the network of gold tetrahedra. LMTO band structure calculations reveal metallic properties and a pseudogap at 256 valence electrons per formula unit, only three electrons fewer than in the title compound and at a point at which strong Au−Sn bonding is optimized. Additionally, the tight coordination of the Au framework atoms by K plays an important bonding role: each Au tetrahedra has 10 K neighbors and each K atom has 8−12 Au contacts. The appreciably different role of the p element Sn in this structure from that in the triel members in K_3Au_5In and Rb_2Au_3Tl appears to arise from its higher electron count which leads to better p-bonding (valence electron concentrations = 1.32 versus 1.22).

1. Introduction

The formation of compounds between metals from opposite sides of the periodic table is driven by intimately related factors, such as delocalized bonding, high coordination numbers, and differences in electronegativity (*EN*). For larger *EN* differences, *Zintl* phases[1,2] between electropositive elements and closed shell polyanions often form. Combinations of different p metals and/or active metals in multinary systems have been a fruitful route to new and diverse structures. The bonding in regular *Zintl* phases can be qualitatively assessed by well established electron counting rules, which include the octet concept and Wade's rules[3] for polyhedral building blocks in moderately electron-poor systems with partially delocalized bonds. However, the delicate interplay between different energy terms often demands, even in these "extreme" intermetallic cases, more critical ways of structure interpretation.

In recent years, this highly exploratory research has been substantially extended to electron-poorer systems by the inclusion of earlier p[2,4] or late d[5] elements in moderate amounts. With gold, very stable and even electron-poorer systems are realized, and the deployment of its unique electronic properties[6] has frequently led to new structures with novel bonding.[7] Gold-rich systems are of particular interest inasmuch as both very low valence electron concentrations (*vec*), and substantial involvement of its $5d^{10}$ shell in bonding (through relativistic effects) can be achieved. These approach the region of typical intermetallic systems, such as Hume−Rothery "electron" phases (*vec* < 2, neglecting d^{10})[8] but at the same time the high *EN* of Au suggests rather polar bond characteristics with other metals. This phase region often features non-classical arrangements, such as icosahedral quasicrystals and approximants,[7a] quasi-infinite tunnel structures,[7b,c] networks of cation-centered polyhedra,[7d] and

*To whom correspondence should be addressed. E-mail: jcorbett@iastate.edu.

(1) Schäfer, H.; Eisenmann, B.; Müller, W. *Angew. Chem., Int. Ed. Engl.* **1973**, *12*, 694.
(2) *Chemistry, Structure and Bonding of Zintl Phases and Ions*; Kauzlarich, S., Ed.; VCH Publishers: New York, 1996; Chapter 3.
(3) Wade, K. *Adv. Inorg. Chem. Radiochem.* **1976**, *18*, 1.
(4) Vaughey, J. T.; Corbett, J. D. *J. Am. Chem. Soc.* **1996**, *118*, 12098.
(5) (a) Kim, S.-J.; Hoffmann, S. D.; Fässler, T. F. *Angew. Chem., Int. Ed.* **2007**, *46*, 3144. (b) Xia, S.; Bobev, S. *J. Am. Chem. Soc.* **2007**, *129*, 4049. (c) Todorov, E.; Sevov, S. C. *Angew. Chem., Int. Ed.* **1999**, *38*, 1775.
(6) (a) Pyykkö, P. *Chem. Rev.* **1988**, *88*, 63. (b) Pyykkö, P. *Angew. Chem., Int. Ed.* **2002**, *41*, 3573. (c) Pyykkö, P. *Chem. Soc. Rev.* **2008**, *37*, 1967.
(7) (a) Lin, Q.; Corbett, J. D. *J. Am. Chem. Soc.* **2007**, *129*, 6789. (b) Li, B.; Corbett, J. D. *Inorg. Chem.* **2007**, *46*, 6022. (c) Sinnen, H. D.; Schuster, H. U. *Z. Naturforsch.* **1978**, *33B*, 1077. (d) Li, B.; Corbett, J. D. *Inorg. Chem.* **2008**, *47*, 3610.
(8) (a) Miller, G. J.; Lee, C.-S.; Choe, W. In *Inorganic Chemistry Highlights*; Meyer, G., Naumann, D., Wesemann, L., Eds.; Wiley-VCH Verlag-Gmbh: Weinheim, Germany, 2002; Chapter 2.(b) Mizutani, U.; Takeuchi, T.; Fournée, V.; Sato, H.; Banno, E.; Onogi, T. *Scripta Mater.* **2001**, *44*, 1181.

 Published on Web 10/29/2009

gold sublattices built at least in part of tetrahedral Au_4 units.[9,10] These examples show that this region may have not only particular *vec* criteria but also strong influences of atomic sizes and the often unappreciated and underestimated cation−anion interactions in the lattices.[11] Together, these collective aspects render such electron-poor intermetallic systems challenging to understand, ultimately because of a lack of closed shell or other clear valence rules.

Recently, we reported the phases A_3Au_5Tr and A_2Au_3Tl (A = K, Rb; Tr = In, Tl)[10] in which segregation (clustering) of the different heavy elements is dominant, and Au−Tr bond optimization is not accomplished. Within this context, we have also investigated compositionally similar A−Au−Sn systems aimed at the study of combined Au clusterings and more *Zintl*-like behavior of the tetrels (Si − Pb). Particularly Sn, as well as Ge, frequently form 2*c*−2*e* bonds in intermetallic systems, and most of the known A−Sn binary phases follow *Zintl* concepts.[12] Up to now, the gold-rich region of this ternary system includes K_3Au_5Pb[9e] and $A_4Au_7Tt_2$ (A = K−Cs, Tt = Ge, Sn).[9a−c] The former contains infinite layers of vertex sharing Au tetrahedra linked by zigzag chains of Pb, as in K_3Au_5Tr, and the latter, pairs of gold tetrahedra that are linked by Tt_2 dimers. Herein, we report the synthesis, structure, and bonding of $K_{12}Au_{21}Sn_4$, a new structure type that contains building units of *Laves* and zinc blende type structures with two contrasting gold functionalities.

2. Experimental Section

Synthesis. All reactants and products were handled in the dry N_2 atmosphere (H_2O level <0.1 ppm) of a glovebox. The procedures followed in part general methods employed before.[7b] Reactions were allowed to take place between weighed amounts of the high purity elements (K: 99.9% (Alfa-Aesar); Au: 99.997% (Ames Lab); Sn: 99.99% (Alfa-Aesar)). These were carried out in a tube furnace with the mixed metals sealed within 9 mm diameter Ta containers that were in turn enclosed in evacuated and well-baked silica jackets to protect the former from air. Initially, $K_{12}Au_{21}Sn_4$ was found in an attempt to obtain the unreported $K_4Au_7Sn_2$. The first reactions followed the sequence of 650 °C for 4 h, cooling at 5 deg/h to 350 °C, equilibration for 160 h, and slow cooling (5 deg/h) to room temperature. Later reactions starting with the composition of the refined structure gave apparent single phase yields of the new $K_{12}Au_{21}Sn_4$ (>95% on the basis of powder pattern data). The compound is silvery with metallic luster and moderately sensitive to moisture (judging from a single crystal exposed to air). EDS measurements on a single crystal, using a Jeol 5910LV scanning electron microscope (20 kV) and a Noran−Vantage detector, confirmed the presence of only K, Au, and Sn in the proportions 29.3(6)/59.7(9)/11.0(9) (calculated: 32.4/56.8/10.8). Attempts to synthesize up to three-electron-poorer isotypes from loadings such as "$K_{12}Au_{21}Sn_{4-x}In_x$ (x = 2, 2.5, 3)", were unsuccessful and, according to powder X-ray diffraction (XRD) measurements, led to phase mixtures containing mainly K_3Au_5In[10] plus unknown side products.

Table 1. Selected Crystal and Structure Refinement Data for $K_{12}Au_{21}Sn_4$

empirical formula	$K_{12}Au_{21}Sn_4$
fw/g·mol^{-1}	5080.26
space group, Z	*Pmmn* (No.59), 2
unit cell parameters	
a	12.162(2) Å
b	18.058(4) Å
c	8.657(2) Å
V	1901.3(7) Å^3
ρ_{calc}/g·cm^{-3}	8.87
μ/mm^{-1} (Mo Kα)	84.5
R_1/wR_2 [$I > 2\sigma(I)$]	0.047/0.105
R_1/wR_2 [all data]	0.074/0.115

X-ray Diffraction Studies. Powder diffraction data were collected with the aid of a Huber 670 Guinier powder camera equipped with an area detector and Cu $K\alpha_1$ radiation (λ = 1.540598 Å). The samples were homogeneously dispersed in a glovebox between two Mylar sheets with the aid of a little vacuum grease. These, in turn, were held between split Al rings that provided airtight seals. Unit cell parameters were refined from these data with the WinXPow program,[13] values of which were subsequently used for the distance calculations from single crystal structural data.

Single crystal diffraction data sets were collected at 293(2) K with Mo−K_α radiation (λ = 0.71073 Å) and a Bruker Apex I diffractometer. The data came from three sets of 606 frames, each with 0.3° scans in ω and exposure times of 10 s per frame. Space group determination was done with the aid of the XPREP program included in the SHELXTL 6.1 software package.[14] A numerical absorption correction was applied according to X-Red and X-Shape from the X-Area package[15] and with good results. The structure was then solved by direct methods with the aid of SHELXTL 6.1 and subsequently refined in the indicated centrosymmetric space group *Pmmn* (origin choice 2) by full-matrix least-squares on F_o^2, ultimately with anisotropic displacement parameters. The unusual 4*b*-Au8 showed a slightly higher U_{eq} value (24 Å^2 × 10^{-3}) relative to its bonded Sn neighbors (13−14) and the other Au (15−19). However, refinements with mixed atoms or free occupancy factors did not alter the structural results. Mixed refinement of Au8 with Sn resulted in an occupancy factor of 0.97(2) Au. Therefore, we exclude the presence of Sn−Sn interactions; rather the higher U_{eq} seems to originate more from the open environment around Au8 (below). Some data collection and refinement parameters are collected in Table 1, the atom positional data for the structure are given in Table 2, and important bond distances are listed in Table 3. The cif output and detailed tabular material are provided in the Supporting Information.

Electronic Structure Calculations. Tight-binding electronic structure calculations were performed according to the linear muffin-tin-orbital (LMTO) method in the atomic sphere approximation (ASA).[16] The radii of the Wigner-Seitz (WS) spheres were assigned automatically so that the overlapping potentials would be the best possible approximations to the full potentials.[17] No interstitial (empty) spheres were necessary for space filling in the atomic sphere approximation within a limit of 18% overlap with any atom-centered sphere. WS radii [Å] were

(9) (a) Sinnen, H.-D.; Schuster, H.-U. *Z. Naturforsch.* **1981**, *36b*, 833. (b) Zachwieja, U. *Z. Anorg. Allg. Chem.* **1995**, *621*, 975. (c) Zachwieja, U.; Wlodarski, J. *Z. Anorg. Allg. Chem.* **1998**, *624*, 1443. (d) Müller, J.; Zachwieja, U. *Z. Anorg. Allg. Chem.* **2000**, *626*, 1867. (e) Zachwieja, U.; Wlodarski, J. *Z. Anorg. Allg. Chem.* **1998**, *624*, 1569.

(10) Li, B; Kim, S.-J.; Miller, G. J.; Corbett, J. D. *Inorg. Chem.* **2009**, *48*, 6573.

(11) (a) Li, B.; Corbett, J. D. *Inorg. Chem.* **2005**, *44*, 6515. (b) Mudring, A.-V.; Corbett, J. D. *J. Am. Chem. Soc.* **2004**, *126*, 5277. (c) Mudring, A.-V.; Corbett, J. D. *Inorg. Chem.* **2005**, *44*, 5636. (d) Li, B.; Mudring, A.-V.; Corbett, J. D. *Inorg. Chem.* **2003**, *42*, 6940.

(12) Fässler, T. F. *Z. Anorg. Allg. Chem.* **2007**, *632*, 1125, and references therein

(13) *WinXPow 2.10*; Stoe & Cie GmbH: Darmstadt, Germany, 2004.

(14) *SHELXTL 6.1*; Bruker AXS, Inc.: Madison, WI, 1996.

(15) (a) *X-Red: Stoe Data Reduction Program*, Version 1.22; Stoe & Cie GmbH: Darmstadt, Germany, 2001. (b) *X-Shape: Crystal Optimization for Numerical Absorption Correction*, Version 1.06; Stoe & Cie GmbH: Darmstadt, Germany, 1999.

(16) Krier, G.; Jepsen, O.; Burkhardt, A.; Andersen, O. K. *TB-LMTO-ASA Program*, Vers. 4.7; Max-Planck-Institut für Festkörperforschung: Stuttgart, Germany, 1995.

(17) Jepsen, O.; Andersen, O. K. *Z. Phys. B* **1995**, *97*, 35.

Table 2. Atomic Coordinates and Equivalent Isotropic Displacement Parameters ($Å^2 \times 10^3$) for $K_{12}Au_{21}Sn_4$

atom	Wyckoff	*x*	*y*	*z*	U_{eq}[a]
Au1	4*e*	1/4	0.1693(1)	0.5794(1)	17(1)
Au2	8*g*	0.1355(1)	0.0859(1)	0.8024(1)	15(1)
Au3	4*e*	1/4	0.0156(1)	0.5641(1)	16(1)
Au4	4*f*	0.1378(1)	1/4	0.3542(1)	19(1)
Au5	8*g*	0.0912(1)	0.5856(1)	0.2333(1)	17(1)
Au6	4*c*	0	0	0	17(1)
Au7	8*g*	0.0026(1)	0.1515(1)	0.0256(1)	19(1)
Au8	2*b*	1/4	3/4	0.5899(2)	24(1)
Sn1	4*e*	1/4	0.6154(1)	0.4282(2)	13(1)
Sn2	4*f*	0.9406(2)	1/4	0.2285(2)	14(1)
K1	8*g*	0.0085(4)	0.0794(3)	0.3954(6)	21(1)
K2	4*e*	1/4	0.0740(4)	0.1725(9)	28(2)
K3	4*e*	1/4	0.5865(4)	0.8781(8)	22(2)
K4	4*f*	0.9990(7)	1/4	0.6711(9)	25(2)
K5	2*b*	1/4	3/4	0.112(1)	26(2)
K6	2*a*	1/4	1/4	0.962(1)	26(2)

[a] U_{eq} is defined as one-third of the trace of the orthogonalized U_{ij} tensor.

Table 3. Selected Bond Distances [Å] for $K_{12}Au_{21}Sn_4$ and −ICOHP Values [eV/bond·mol]; *n* is the Number of Interactions of Each Type per Unit Cell[a]

atom pair	*n*	distance	−ICOHP	atom pair	*n*	distance	−ICOHP
Au1−Au3	2	2.778(2)	1.27	Au5−Au6	4	2.775(1)	1.25
Au1−Au4	4	2.791(2)	1.26	Au5−Au7	4	2.783(1)	1.35
Au1−Au2	4	2.817(1)	1.02	Au6−Au7	4	2.746(1)	1.31
Au1−Au1	2	2.914(2)	0.85	Au3−Sn1	4	2.643(2)	2.82
Au2−Au5	4	2.774(1)	1.35	Au4−Sn2	4	2.634(2)	2.79
Au2−Au7	4	2.784(1)	1.29	Au5−Sn1	8	2.620(2)	2.90
Au2−Au2	4	2.785(2)	1.07	Au7−Sn2	8	2.611(2)	2.80
Au2−Au3	4	2.794(1)	1.24	Au8−Sn2	4	2.800(2)	2.25
Au2−Au6	4	2.837(1)	1.02	Au8−Sn1	4	2.805(2)	2.32
Au4−Au4	2	2.729(2)	1.61	K−Au	248	3.22−3.92	av. 0.19
				K−Sn	48	3.47−3.98	av. 0.23

[a] Au−Au: Au−Sn: K−Au: K−Sn bonds occur as 46: 32: 248: 48 in the unit cell.

as follows: K, 1.95−2.00; Au, 1.52−1.66; Sn, 1.58. The calculations utilized a basis set of K 4s/(4p)/3d, Au 6s/6p/5d/(5f), Sn 5s/5p/(4d/4f) (downfolded[18] orbitals in parentheses), and reciprocal space integrations were performed on a grid of 64 irreducible *k* points. Scalar relativistic corrections were included. For bonding analysis, the energy contributions of all electronic states for selected atom pairs were calculated by the crystal orbital Hamilton populations (COHP) method.[19] Integration over all filled states yielded −ICOHP values as measures of relative overlap populations. COHP diagrams are necessarily drawn as −COHP versus *E* inasmuch as the former represents bonding interactions.

3. Results and Discussions

Crystal Structure. $K_{12}Au_{21}Sn_4$ crystallizes in a new structure type (*Pmmn*) with Pearson code *oP*74. The unit cell, Figure 1a, contains two distinctive motifs: Au_4 tetrahedra that are connected at two or three shared vertices into sheets and, embedded therein, network fragments of four 4*b*-Sn atoms (blue) centered by 4*b*-Au8 (orange). The K atoms (red) efficiently fill the holes of the 3D structure. We note that $K_{12}Au_{21}Sn_4$ retains the

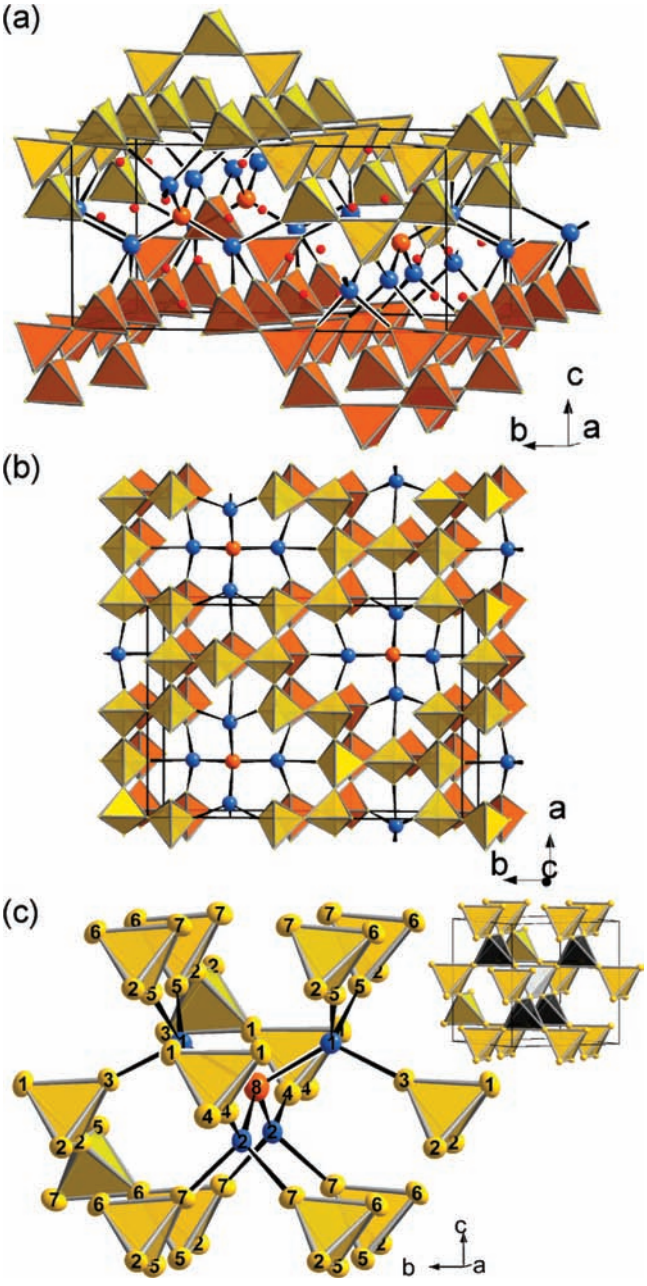

Figure 1. General views of $K_{12}Au_{21}Sn_4$ along (a) ~[100] and (b) ~[001]. Two equivalent wavy sheets of vertex-sharing Au tetrahedra are shown in yellow and orange. They are tied together by a sheet of 4*b*-Au8 (orange), -Sn1, and -Sn2 (blue). (c) An enlarged view around an Au8 atom (95% ellipsoids) and the corresponding section of $NaAu_2$ (inset). The light and dark gray tetrahedra in the latter mark the Au8 and Sn substitution sites, respectively.

motif of condensed gold tetrahedra that occur in simple binaries, such as in AAu_2 (A = Na, K),[20] Rb_3Au_7,[21] AAu_5 (A = K, Rb),[22] as well as in ternary examples, such as K_3Au_5M (M = In, Tl, Pb)[9e,10] and Rb_2Au_3Tl.[10] These and the seeming avoidance of element mixing on any site suggest high stability and flexible Au_4 clustering.

(18) (a) Lambrecht, W. R. L.; Andersen, O. K. *Phys. Rev. B* **1986**, *34*, 2439. (b) Löwdin, P. *J. Chem. Phys.* **1951**, *19*, 1396.
(19) Dronskowski, R.; Blöchl, P. E. *J. Phys. Chem.* **1993**, *97*, 8617.
(20) (a) Haucke, W. *Naturwissenschaften* **1937**, *25*, 61. (b) Zachwieja, U. *J. Alloys Cmpd.* **1993**, *196*, 171. (c) Range, K. J.; Rau, F.; Klement, U. *Acta Crystallogr., Sect. C* **1988**, *44*, 1485.
(21) Zachwieja, U. *J. Alloys Compd.* **1993**, *199*, 115.
(22) Raub, C. J.; Compton, V. B. *Z. Anorg. Allg. Chem.* **1964**, *332*, 5.

The gold tetrahedra in $K_{12}Au_{21}Sn_4$ are bonded within infinite corrugated sheets around the *ab* plane, Figure 1a. Two such sheets, shown in yellow and orange for contrast, are related by an *n* glide plane at $z = 0, 1/2$ and do not have direct bonds between them. Rather, they are connected via single sheets of 4*b*-Sn (blue) and the special Au8 atoms (orange) that define rough tunnels along *c*, Figure 1b. As shown in better detail in Figure 1c the Au8 atoms (*mm*2 site symmetry) are approximately tetrahedrally coordinated by 2× Sn1 (at 120°) and 2× Sn2 (at 112°) atoms. The valence angles at Sn are only ~86−96° toward bound vertices of the Au_4 tetrahedra. Thereby, each Sn atom links two Au_4 tetrahedra from one sheet (Sn1−Au5 or Sn2−Au7) plus one Au_4 unit from an adjacent sheet below (Sn1−Au3) or above (Sn2−Au4). (A similar $SnIn_4^{8+}$ unit resembling the $AuSn_4$ group in this work is present in In_4SnS_4.[23]) The two last Sn−Au8 bond distances about the two Sn are substantially the same (~2.80 Å) but significantly longer than to the exobonded (exo*b*-) Au atoms that line the Au tetrahedral network (2.61−2.64 Å). Both distance sets are in the range found in organometallic molecules,[24] and the shorter compare well with the sum of covalent radii.[25] The more open environment around 4*b*-Au8 is unusual relative to that in many other gold networks, both in its larger distances to Sn and larger U_{eq} value (0.024 $Å^2$). These parallels presumably reflect different bonding characteristics among the Au−Sn contacts, although bond distances alone are often the least significant indicators.

The structure of $K_{12}Au_{21}Sn_4$ shows a significant close relationship to the cubic *Laves* structure[26] of $NaAu_2$[20a,b] and to its ternary derivatives A_3Au_5M (A = K, Rb; M = In, Tl, Pb)[9e,10] and Rb_2Au_3Tl[10] via an atom-for-cluster replacement. Certain centered supertetrahedra in $NaAu_2$, the five gray Au tetrahedra in the inset of Figure 1c, are replaced by [$AuSn_4$] fragments. Overall, this substitution affects one in six Au atoms as these five atoms replace a net of four Au atoms so that a 12:(24 + 1) stoichiometry is achieved relative to the 1:2 *Laves* proportion. In contrast to the segregation of Tr/*Tt* atoms into zigzag chains in K_3Au_5In, and so forth, the Sn atoms have only Au neighbors, but nearly the same Au:*M* proportions and *vec* (1.22 versus 1.32, counted over all atoms but without $5d^{10}$ shells). The separation into more classical (4*b*) fragments here further contrasts with that in other gold-rich phases, such as KAu_4Sn_2[7c] and Ca−Au−Sn,Ge[27] systems with similar *vec* but less open networks. In $K_{12}Au_{21}Sn_4$, tetrahedral building blocks seen in *Laves* phases as well as 4*b*-zinc blende like fragments (such as in Half-Heusler phases), occur within one structure. This means, hierarchically, that the structure can also be understood as a NaTl[28] derivative (Supporting Information, Figure S2).

The homoatomic gold substructure consists of three types of linked tetrahedra ***A***, ***B***, and ***C*** in 1:2:4 proportions, as shown in Figure 2a. The tetrahedra share two or three vertices (as 6*b*-Au), whereas the remaining vertices (exo*b*-Au) bond to Sn, and thus contain totals of 3, 2.5, and 3 Au atoms, namely, ***A***: $\{(Au1)_{2/2}(Au4)_{2/1}\}$, ***B***: $\{(Au1)_{1/2}(Au2)_{2/2}Au3_{1/1}\}$, and ***C***: $\{(Au2)_{1/2}Au5_{1/1}(Au6)_{1/2}\ Au7_{1/1}\}$), respectively. Internal distances in the range of 2.73−2.92 Å, Table 3, span those of the bulk gold (2.88 Å), and the Au−Au−Au angles are around 60 ± 3° (or multiples thereof).

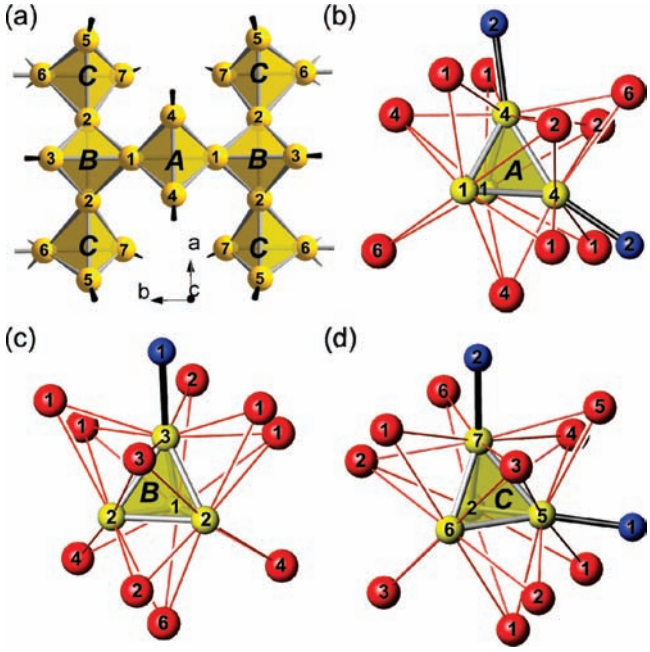

Figure 2. Further structural details in $K_{12}Au_{21}Sn_4$: (a) The condensation modes of the different tetrahedra, the broken black *exo*-bonds marking connections to Sn. (b−d) The three different Au_4 tetrahedra (***A***−***C***) are tightly surrounded by 10 K atoms that cap all faces and edges.

As might be expected for such a complex polar structure, the six independent K atoms are tightly and uniformly bound primarily to the network of Au tetrahedra. Ten K atoms collectively bridge all six Au−Au edges and cap all triangular faces on each of the three types of tetrahedra, Figure 2b−d. In turn, the cations all have relatively symmetric environments and high coordination numbers (≤4 Å, Supporting Information, Figure S1): The K2 and K6 are each surrounded by 12 Au neighbors, in a pattern reminiscent of a truncated tetrahedron, whereas the other four have 10−8 plus 2−4 contacts with Au and Sn atoms, respectively (d(K−Au) = 3.47−3.72 Å; d(K−Sn) = 3.53−3.95 Å).

Electronic Structure and Bonding. The electronic densities of states (DOS) and −COHP plots for $K_{12}Au_{21}Sn_4$ (from the LMTO band structure calculations) are provided in Figure 3. The total DOS features a broad valence band, but the characteristics of a metallic conductor are still present. This transport property is clearly 3D, as band crossings occur along every direction throughout the irreducible wedge of the first Brillouin zone (Supporting Information, Figure S3). However, a deep pseudogap (with a very low but finite DOS) at 512 e^-/cell (Z = 2) around −0.5 eV indicates some additional features of the bonding. Under rigid band assumptions, moderate substitution with electron-poorer elements, for example, three In for three Sn per f.u., might be possible, but the stability of an alternative phase dominates with the

(23) Deiseroth, H. J.; Pfeifer, H. *Z. Kristallogr.* **1991**, *196*, 197.
(24) Gade, L. H. *Eur. J. Inorg. Chem.* **2002**, 1257.
(25) Atsumi, M.; Pyykkö, P. *Chem.−Eur. J.* **2009**, *15*, 186.
(26) (a) Friauf, J. B. *J. Am. Chem. Soc.* **1927**, *49*, 3107. (b) Friauf, J. B. *Phys. Rev.* **1927**, *29*, 34.
(27) Lin, Q.; Corbett, J. D. *Inorg. Chem.* **2009**, *48*, 5403.
(28) Zintl, E.; Dullenkopf, W. *Z. Phys. Chem.* **1932**, *16*, 195.

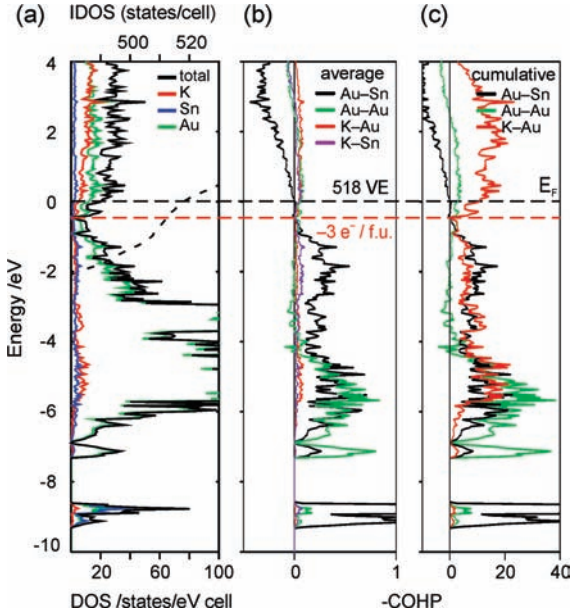

Figure 3. TB−LMTO−ASA electronic structure results for $K_{12}Au_{21}Sn_4$: (a) Total DOS (black) and partial DOS curves for K (red), Au (green), and Sn (blue). (b) Average COHP results for Au−Au, Au−Sn, K−Au, and K−Sn interactions. (c) Cumulative COHP data considering bond multiplicities. The Fermi level (518 e^-, $Z = 2$) and the pseudogap (512 e^-) are marked with black and red dashed lines, respectively.

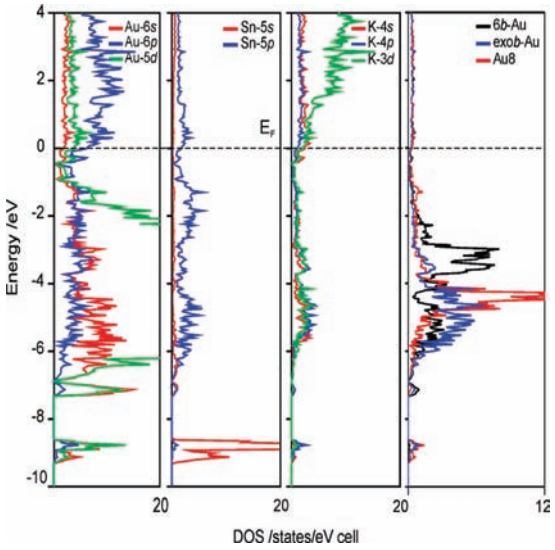

Figure 4. Orbital components to the DOS for the constituent elements and the DOS of different Au atom types (per atom) in $K_{12}Au_{21}Sn_4$.

formation of the nearby K_3Au_5In ($= K_{12}Au_{20}In_4$) which lacks only the "odd" Au8 equivalent (Experimental Section).

The orbital contributions of each constituent element (Figure 4) show that most of the Au valence s and d, and part of the p orbitals are filled, which suggests negative oxidation states for Au. The 6p/6s IDOS ratios (at E_F) decrease in the order 4*b*-Au8, 6*b*-Au, and exo*b*-Au (Supporting Information, Table S4, Figure S4), reflecting electron-poor bonding within and nearly normal bonding outside of the gold tetrahedra. Particularly the Au 6s contributions fall within the energy range of the dominant Au 5d bands, which are effectively raised by relativistic effects.[8] Further, the small differentiation among the 5d states reflects effective orbital degeneracies, in spite of the different chemical environments, of the 6*b*- ($\sim D_{3d}$) and the exo*b*-Au atoms ($\sim C_{3v}$), Figure 4, right. In contrast, the 5d band for 4*b*-Au8 is rather confined at about −4.5 eV and shows little crystal splitting. The valence states for Sn are distinctively split into a narrow core-like 5s band and a broad 5p band, whereas the small contributions of K to the DOS are almost equally distributed among 4s, 4p, and neighboring 3d functions (Figure 4).

Table 4. Individual and Cumulative −ICOHP Components (eV) in $K_{12}Au_{21}Sn_4$

	Au−Au	Au−Sn	K−Au	K−Sn
−ICOHP (per bond·mol)	1.22	2.70	0.19	0.23
no. of bonds per unit cell ($Z = 2$)	46	32	248	48
−ICOHP (cumulative, per cell)	56.1	86.4	47.1	11.0
%	28	43	23	5

Crystal orbital Hamilton populations (−COHP) and their energy-weighted integrals up to E_F, −ICOHP, (Figure 3b,c, Table 3) allow comparison of bonding energies. The Au−Au bonding is significant up to 4 eV, over the lower part of the Au 5d band, whereas Au−Sn is effective over the whole region. The average −ICOHP value for each bond type and the sum for each over the whole cell are compared in Table 4. The average Au−Sn interaction is the largest, 2.70 eV(·mol), relative to Au−Au, 1.22 eV, and the average K−Au and K−Sn values are naturally smaller, 0.19 and 0.23 eV, respectively. Thus, strong homo− and heteroatomic bonding pertains over the whole $[Au_{21}Sn_4]$ network. However, consideration of bond multiplicities as well (or semiquantitative cumulative COHP diagrams, Figure 3c) shows that the overall contribution of K to the bonding is significant. The numbers of Au−Au:Au−Sn:K−Au:K−Sn bonds per cell are 46:32:248:48, making the cumulative −ICOHP values 56.1, 86.4, 47.1, and 11.0 eV, respectively. If we give these approximately equal weights, the contributions to bonding in this solid are something like Au−Au, 28%; Au−Sn, 43%; K−Au, 23%; K−Sn, 5%. The numerical dominance of the (nonpolar) Au−Au contacts give way to the distinctly larger value for the polar Au−Sn components, and the under-recognized K−Au result is rather new. Comparison of these data with those for K_3Au_5Tr[10] is especially distinctive, as for the two structures. Average values of −ICOHP for the principal bonding pairs, Au−Sn and Au−Au here versus Au−Tr and Au−Au are about 23% larger and 10% smaller, respectively, and the relative number of heteroatomic bonds, Au−Sn versus Au−Tr, have about doubled. Thus the bottom line: the percentages of the total bond populations by these measures have fallen by ∼30% for Au−Au but increased by ∼100% for Au−Sn, Table 4. These are in accord with what one sees in the structural changes, a transformation of the entire significant fraction of Tr−Tr chain bonding into heteroatomic Au−Sn bonds. One steady feature remains; the many K−Au contacts make up 23% of the total ICOHP here compared with 24% in the rather different K_3Au_5Tr structure. The high structural preference for the observed Au−Sn distribution was independently confirmed by evaluation of the total energy[29]

(29) Total energy values were obtained from pseudopotential calculations using the Vienna ab initio Simulation Package VASP.[30] The calculations converged to less than 1 meV per unit cell.

of alternative constitutions. Model structures with one Au in the network switched with a Sn1 or Sn2 site resulted in total energy changes of +1.71 or +1.68 eV/f.u. relative to the observed structure.

Generally, the formation of tetrahedra, at the given alkali-metal-poor proportions, is expected rather than chains, rhombi, or squares (all of which occur in alkali-metal-richer binary aurides). This feature maximizes the number of nearest neighbor bonds.[31] Optimal chemical bonding in isolated tetrahedra of main group elements occurs for 20 cluster electrons (six skeletal 2*c*−2*e* bonds plus four lone pairs), as seen in Tr_4^{8-}, Tt_4^{4-}, and Pn_4. Not nearly as many valence electrons are available for Au, and four skeletal molecular orbitals (MOs) are sufficient, of which the low lying a_1 highest occupied molecular orbital (HOMO) and three higher and empty t_2 orbitals give rise to $\{Au_4\}^{2+}$.[32] Molecular ligated Au_4 units are in agreement with that bonding model.[33] Upon condensation into the solid, the molecular states broaden to bands and, ultimately, the available electrons lead to filling of 6p states. In $K_{12}Au_{21}Sn_4$ the significant Au−Au bonding fraction of the COHP coincides with the maximum DOS of Au 6s, Figure 4, suggesting the filling of strong 6s−6s bonding, 6s−6s antibonding, and weaker 6s−6p and 6p−6p bonding states as well. (Of course, special electronic properties of electron-poorer gold make its 5d orbitals major contributors to the overall bonding too.) Further hints toward two electrons per tetrahedron have been extracted for related golden cages.[34]

On the other hand, optimization of the Au−Sn bonds is substantially accomplished, mainly bonding states occur below E_F, and the region between E_F and the pseudogap contains nearly nonbonding Au−Sn states. However, the −COHP curves for the two different Au−Sn interactions (exo*b*-Au vs 4*b*-Au8) are different: The short exo*b*-Au−Sn bonds (∼2.63 Å) stem from larger contributions from Au/Sn s orbitals around −9 eV, whereas the longer Au8−Sn (∼2.82 Å) bonds are more evenly distributed among s and p functions. Distancewise, the latter are more comparable to those in the *Zintl* phases K_3AuSn_4,[35] $K_4Au(TlSn_3)$,[36] and the complex condensed networks of augmented trigonal prismatic units of $KAu_{10}Sn_{10}$.[7d] The Au 5d involvement in Au−Sn bonding is low, especially for Au8 for which its narrow DOS d peak (Figure 4) has no correspondence in the COHP diagram. The DOS of Au8 suggests and approaches that of a reduced "Au^{3-}" ($d^{10}s^2p^2$), which is isovalent with a tetrel element. An Au^+ ($d^{10}s^0p^0$), despite its acceptable tetrahedral coordination, seems to be less likely considering the significant filling of 6s/p states.

In the simplest view, two bonding electrons per tetrahedron in the gold network[32,34] together with 2*c*-2*e* bonds in the open 4-bonded zinc blende portion yield the 256-e count for $K_{12}Au_{21}Sn_4$ at the observed pseudogap, as before.[10] The three additional electrons per formula unit present are clearly related to the significant K−Au bonding. Accordingly, any comprehensive understanding of the electronic structure of such compounds using only conventional electron counting schemes must remain approximations.

Conclusions

A substantial segregation of the elements into homoatomic substructures is observed in K_3Au_5Tr ($K_{12}Au_{20}Tr_4$) and Rb_2Au_3Tl ($Rb_{12}Au_{18}Tl_6$),[10] in which the Tr are also 4-bonded. Although $K_{12}Au_{21}Sn_4$ contains a similar vertex-sharing Au_4 motif, the main group element Sn participates only in a 4*b*-heteroatomic substructure. The arrangement effectively maximizes the number of heteroatomic contacts and, simultaneously, the higher *vec* (1.32, omitting $5d^{10}$) leads to effective filling of the bonding Au−Sn states, whereas not enough electrons are present to do likewise in K_3Au_5Tr (*vec* = 1.22). Furthermore, the novel coexistence of the strongly condensed gold tetrahedra and the rather open classical diamond type network within one structure emphasizes the stability of the tetrahedral Au backbone.

Acknowledgment. This research was supported by the Office of the Basic Energy Sciences, Materials Sciences Division, U.S. Department of Energy (DOE) and was carried out in the facilities of Ames Laboratory. The Ames Laboratory is operated for DOE by Iowa State University under contract No. DE-AC02-07CH11358.

Supporting Information Available: Single crystal refinement data in CIF format; detailed tables and figures with further crystallographic data, and structural details; band dispersions; further breakdowns of LMTO band structure outputs. This material is available free of charge via the Internet at http://pubs.acs.org.

(30) (a) Kresse, G.; Hafner, J. *Phys. Rev. B* **1993**, *47*, 558. (b) Kresse, G.; Furthmüller, J. *Comput. Mater. Sci.* **1996**, *6*, 15.
(31) *Bonding and Structure of Molecules and Solids*; Pettifor, D. G., Ed.; Clarendon Press : Oxford, 1995.
(32) Mingos, D. M. P. In *Gold: Progress in Chemistry, Biology and Technology*; Schmidbaur, H., Ed.; Wiley: Chichester, U.K., 1999.
(33) Evans, D. G.; Mingos, D. M. P. *J. Organomet. Chem.* **1982**, *232*, 171.
(34) Zubarev, D. Y.; Boldyrev, A. L. *J. Phys Chem. A* **2009**, *113*, 866.
(35) Zachwieja, U.; Müller, J.; Wlodarski, J. *Z. Anorg. Allg. Chem.* **1998**, *624*, 853.
(36) Huang, D.; Corbett, J. D. *Inorg. Chem.* **1998**, *37*, 5007.